

Dynamics of the Innermost Accretion Flows Around Compact Objects: Magnetosphere-Disc Interface, Global Oscillations and Instabilities

Wen Fu^{1,2*} and Dong Lai^{1*}

¹*Department of Astronomy, Cornell University, Ithaca, NY 14853, USA*

²*Theoretical Division, Los Alamos National Laboratory, Los Alamos, NM 87545, USA*

18 October 2018

ABSTRACT

We study global non-axisymmetric oscillation modes and instabilities in magnetosphere-disc systems, as expected in neutron star X-ray binaries and possibly also in accreting black hole systems. Our two-dimensional magnetosphere-disc model consists of a Keplerian disc in contact with a uniformly rotating magnetosphere with low plasma density. Two types of global overstable modes exist in such systems, the interface modes and the disc inertial-acoustic modes. We examine various physical effects and parameters that influence the properties of these oscillation modes, particularly their growth rates, including the magnetosphere field configuration, the velocity and density contrasts across the magnetosphere-disc interface, the rotation profile (with Newtonian or pseudo General Relativistic potential), the sound speed and magnetic field of the disc. The interface modes are driven unstable by Rayleigh-Taylor and Kelvin-Helmholtz instabilities, but can be stabilized by the toroidal field (through magnetic tension) and disc differential rotation (through finite vorticity). General relativity increases their growth rates by modifying the disc vorticity outside the magnetosphere boundary. The interface modes may also be affected by wave absorption associated with corotation resonance in the disc. In the presence of a magnetosphere, the inertial-acoustic modes are effectively trapped at the innermost region of the relativistic disc just outside the interface. They are driven unstable by wave absorption at the corotation resonance, but can be stabilized by modest disc magnetic fields. The overstable oscillation modes studied in this paper have characteristic properties that make them possible candidates for the quasi-periodic oscillations observed in X-ray binaries.

Key words: accretion, accretion discs – hydrodynamics – MHD – waves – instabilities – X-ray: binaries.

1 INTRODUCTION

Quasi-periodic oscillations (QPOs) in X-ray fluxes, with frequencies comparable to the dynamical frequencies of neutron stars (NSs) and black holes (BHs), have been observed since the 1990s in many X-ray binary systems (e.g., van der Klis 2006), largely thanks to NASA's *Rossi X-ray Timing Explorer* (Swank 1999). They are of great interest because they probe the dynamics of the innermost accretion flows around NSs and BHs, and may potentially help constrain the physics of dense nuclear matter and strong gravity.

The phenomenology of kHz QPOs in NS low-mass X-ray binaries is well established (van der Klis 2006). They usually occur in pairs, with frequencies between 300 Hz and 1.2 kHz, both varying significantly as a function of the X-ray flux. There is some correlation between the upper frequency ν_u and the lower frequency ν_l . Spectral analysis indicates most kHz QPOs arise from variations in the inner disk boundary layers (Gilfanov et al. 2003). High-frequency QPOs (HFQPOs) (40–450 Hz) in BH X-ray binaries have also been intensively studied (Remillard & McClintock 2006; Belloni et al. 2011; Altamirano, Belloni &

* Email: wenfu@astro.cornell.edu (WF); dong@astro.cornell.edu (DL)

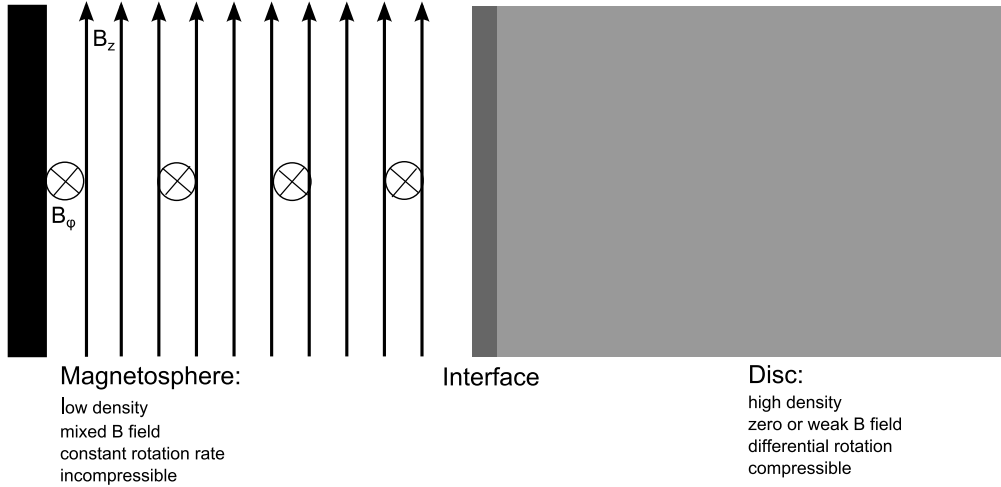


Figure 1. Schematic description of the cylindrical magnetosphere-disc model considered in this paper. The thick black line on the left represents the central compact object. Right next to it is a region of low density plasma threaded by both vertical and toroidal magnetic fields. The disc (on the right) consists of fluid of high density (compared to the magnetosphere) and zero or weak magnetic field. These two regions are separated by a thin interface/boundary layer.

Linares et al. 2011; Altamirano & Belloni 2012), although the signals are much weaker and transient. They are only observed in the “transitional state” (or “steep power law state”) of the X-ray binaries, and have low amplitudes and low coherence. Their frequencies do not vary significantly in response to sizeable (factors of 3-4) luminosity changes. Several systems show pairs of QPOs with frequency ratios close to 2 : 3 (Abramowicz & Kluzniak 2001), 5 : 3 (Kluzniak & Abramowicz 2002), and 5 : 2 (Rebusco, Moskalik & Kluzniak 2012).

Despite much observational progress, the physical origin of HFQPOs remains elusive. Based on the general consensus that HFQPOs are associated with the dynamics of innermost accretion flows, a number of ideas/models with various degrees of sophistication have been proposed or studied. The general notions of hot blobs exhibiting (test-mass) orbital motion and relativistic precession (Stella et al. 1999), nonlinear resonances (Abramowicz & Kluzniak 2001), and in the case of NS systems, beats between the orbital frequency and stellar spin (Miller et al. 1998), have been the most popular among the observers, although it is not clear how these generic ideas are realized in real fluid dynamical models of accretion flows. Other ideas for NS kHz QPOs are discussed in Bachetti et al. (2010). In the case of HFQPOs in BH X-ray binaries, the types of models that go beyond the “test-mass motion” idea are those based on global oscillations of accretion flows, including discs, tori and boundary layers [see below; see also Sect. 1 of Lai & Tsang (2009) for a critical review]. Systematic studies of accretion flow dynamics, combining semi-analytic calculations (for idealized systems to extract physical insights/ingredients) and full numerical simulations (for systems with increasing sophistications and realisms) are essential for making further progress in this field.

In this paper we study a class of models involving global oscillations of inner accretion discs and magnetosphere boundary layers around NSs or BHs. Our model setup (see Fig. 1) consists of an uniformly rotating magnetosphere with both toroidal and poloidal magnetic fields and low plasma density, surrounded by a geometrically thin (Keplerian) disc with high fluid density and zero (or low) magnetic field. To make semi-analytical linear perturbation analysis feasible, our model is two-dimensional with no vertical dependence (i.e., it is height averaged). We consider both Newtonian discs and general relativistic (GR) discs (modelled by the pseudo-Newtonian potential) – we will see that GR can qualitatively affect the linear oscillation modes of the system by changing the disc vorticity profile. This kind of magnetosphere-disc systems can form in accreting NS systems when the NS magnetic field holds off the accretion disc at a certain distance from the stellar surface (e.g., Ghosh & Lamb 1978). They may also be applied to accreting BH systems when magnetic fields advect inwards in the accretion disc and accumulate near the inner edge of the disc (e.g. Bisnovatyi-Kogan & Ruzmaikin 1974, 1976; Igumenshchev, Narayan & Abramowicz 2003; Rothstein & Lovelace 2008, McKinney, Tchekhovskoy & Blandford 2012). It is usually thought that during the “transitional state” (when HFQPOs are observed) of BH X-ray binaries, the accretion flow consists of a thin, thermal disc, truncated by a hot, tenuous (and perhaps highly magnetized) inner corona (e.g., Done et al. 2007; Oda et al. 2010). While the true nature of this flow is unclear, our simple magnetosphere-disc setup may represent an idealization of such a flow.

Loosely speaking, two types of global oscillation modes exist in our 2D magnetosphere-disc systems: *inertial-acoustic modes of the disc* and *interface modes*. Both types of oscillations can be overstable, but driven by different physical mechanisms. Our work represents an extension of related previous studies, which have focused on disc oscillations or interface oscillations separately.

(i) *Disc Oscillations:* Although relativistic fluid discs can support different types of oscillation modes (Okazaki, Kato & Fukue 1987; Nowak & Wagoner 1991; see Wagoner 1999, Kato 2001 and Kato et al. 2008 for reviews), our focus in this paper, as well in our previous papers (Lai & Tsang 2009; Tsang & Lai 2008, 2009c; Fu & Lai 2011a), is on the inertial-acoustic modes (also called p-modes). These modes have no vertical structure (i.e., their wave functions, such as the pressure perturbation, have no node in the vertical direction), and are adequately captured by our 2D model.

On the other hand, our magnetosphere-disc model does not capture other discoseismic modes, including g-modes (also called inertial-gravity modes), c-modes and vertical p-modes (see Wagoner 1999; Kato et al. 2008; Kato 2011a, b). All these modes have vertical structures. Non-axisymmetric g-modes and c-modes are either damped due to corotation resonance (Kato 2003a, Li, Goodman & Narayan 2003; Tsang & Lai 2009a) or their self-trapping zones are easily “destroyed” by disc magnetic fields (Fu & Lai 2009). Although axisymmetric g-modes ($m = 0$) can be resonantly excited by global disc deformations through nonlinear effects (Kato 2003b, 2008; Ferreira & Ogilvie 2008), their trapping zones disappear even for a weak (sub-thermal) disc magnetic field. By contrast, the basic wave properties (e.g., propagation diagram) of p-modes are not strongly affected by disc magnetic fields (Fu & Lai 2009), and it is likely that these p-modes are robust in the presence of disc turbulence (see Arras, Blaes & Turner 2006; Reynolds & Miller 2009).

Our previous papers (Lai & Tsang 2009; Tsang & Lai 2008, 2009c; Fu & Lai 2011a) have shown that non-axisymmetric p-modes trapped in the inner-most region of a BH accretion disc are a promising candidate for explaining HFQPOs in BH x-ray binaries because their frequencies naturally match the observed values without fine-tuning of the disc properties, and because they become overstable due to wave absorption at corotation point when the general relativistic effect on the disc rotation profile is taken into account. Although a toroidal disc magnetic field tends to suppress the instability (Fu & Lai 2011a), a large-scale poloidal field may enhance the instability (Tagger & Pallet 1999; Tagger & Varniere 2006). Most of these previous papers adopt a reflective boundary condition at the inner edge of the disc – this is important for the trapping of disc p-modes (see Lai & Tsang 2009). How such a reflection can be achieved was not clear. We will show in this paper that the disc-magnetosphere boundary serves as a “reflector” for the disc p-modes.

(ii) *Interface Oscillations:* Li & Narayan (2004) were the first to consider the interface modes between a magnetosphere (with a vertical magnetic field) and an incompressible disc in the cylindrical approximation (i.e., no z -dependence). They showed that the interface modes can be subject to Rayleigh-Taylor instability and/or Kelvin-Helmholtz instability, depending on the density contrast and velocity shear across the interface. The mode frequencies roughly scale as $m\Omega_{\text{in}}$, where $m = 1, 2, 3 \dots$ are the azimuthal mode number and Ω_{in} is the angular frequency of the disc flow at the interface, making the interface modes a viable candidate for explaining HFQPOs when the interface radius r_{in} is suitably adjusted. Tsang & Lai (2009b) generalized the analysis of Li & Narayan (2004) by considering compressible discs. They showed that a relatively large disc sound speed is necessary to overcome the stabilizing effect of disc differential rotation and thereby maintain the mode growth. Besides linear calculations, numerical simulations of the magnetosphere-disc interface have also been presented in a number of papers (see Kulkarni & Romanova 2008; Romanova, Kulkarni & Lovelace 2008 and references therein).

One ingredient that has been missing from both Li & Narayan (2004) and Tsang & Lai (2009b) is toroidal magnetic fields in the magnetosphere, which could be a very important component (Ghosh & Lamb 1978; Ikhsanov & Pustil’nik 1996). In this paper, we generalize previous calculations of global non-axisymmetric modes confined near the interface of the magnetosphere-disc system by taking into account toroidal magnetic fields in the magnetosphere. We aim to examine the possibility of large-scale Rayleigh-Taylor/Kelvin-Helmholtz instabilities of the interface in the presence of magnetic fields and disc differential rotation.

Overall, the goal of this paper is to present a complete analysis of large-scale non-axisymmetric modes (including their instabilities) in the magnetosphere boundary and in the surrounding disc, and to assess their viabilities for explaining HFQPOs in accreting compact binaries.

We note that in addition to Li & Narayan (2004) and Tsang & Lai (2009b), our study on the interface modes complements several other works on the instability of magnetized accretion discs. For example, Lubow & Spruit (1995) and Spruit, Stehle & Papaloizou (1995) considered the magnetic interchange instability of a thin rotating disc when a poloidal magnetic field provides some radial support in the disc. Lovelace, Turner & Romanova (2009) studied the instability of a magnetopause for cases where the shear layer has appreciable radial width and found that the Rossby wave instability may arise in the shear layer. Lovelace, Romanova & Newman (2010) considered a setup similar to the present paper, but they included only vertical field in the magnetosphere, and focused on small-scale (with radial wavelength $\ll r$) Kelvin-Helmholtz modes in the boundary layer.

This paper is the fourth in our series of papers on the effects of magnetic fields on the global instabilities of various astrophysical flows, with the previous three focusing on black hole accretion discs (Fu & Lai 2011a), accretion tori (Fu & Lai 2011b) and rotating proto-neutron stars (Fu & Lai 2011c), respectively. Our paper is organized as follows. In Section 2, we present the setup of our cylindrical magnetosphere-disc model and the dynamical equations for wave modes in the model. Section 3 focuses on the interface modes when Newtonian potential is used for disc rotation, while Section 4 deals with both the interface modes and disc p-modes when the GR effect (using pseudo-Newtonian potential) is included in the disc rotation. We discuss our results and conclude in Section 5.

2 EQUILIBRIUM AND PERTURBATION EQUATIONS

We consider a magnetosphere-disc model similar to the one in Tsang & Lai (2009b). It consists of a magnetosphere region where magnetic pressure dominates over gas pressure and a disc region which has high density compared to the magnetosphere (see Fig. 1). These two regions are separated by an interface (boundary layer). Unlike Tsang & Lai (2009b), who considered only vertical magnetic field for the magnetosphere, we take into account both vertical and toroidal fields. In the disc region, gas pressure dominates over magnetic pressure. Since any initial poloidal field is likely to generate a dominating toroidal field due to the disc differential rotation, for simplicity we take the disc to be threaded by toroidal B field only. We assume that flows in both regions are non-self-gravitating, satisfying the usual ideal MHD equations

$$\frac{\partial \rho}{\partial t} + \nabla \cdot (\rho \mathbf{v}) = 0, \quad (1)$$

$$\frac{\partial \mathbf{v}}{\partial t} + (\mathbf{v} \cdot \nabla) \mathbf{v} = -\frac{1}{\rho} \nabla \Pi - \nabla \Phi + \frac{1}{4\pi\rho} (\mathbf{B} \cdot \nabla) \mathbf{B}, \quad (2)$$

$$\frac{\partial \mathbf{B}}{\partial t} = \nabla \times (\mathbf{v} \times \mathbf{B}), \quad (3)$$

where ρ , P , \mathbf{v} are the fluid density, pressure and velocity, Φ is the gravitational potential due to the central compact object, and

$$\Pi \equiv P + \frac{\mathbf{B}^2}{8\pi} \quad (4)$$

is the total pressure. The magnetic field \mathbf{B} also satisfies the equation $\nabla \cdot \mathbf{B} = 0$.

We adopt the cylindrical coordinates (r, ϕ, z) which are centered on the central object and have the z -axis in the direction perpendicular to the disc plane. The unperturbed background disc has a velocity field $\mathbf{v} = r\Omega(r)\hat{\phi}$, and the magnetic field may consist of both toroidal and vertical components $\mathbf{B} = B_\phi(r)\hat{\phi} + B_z(r)\hat{z}$. The gravitational acceleration in radial direction is defined as

$$g = \frac{d\Phi}{dr} \quad (5)$$

so that $-\nabla\Phi = -g\hat{r}$ and $g = r\Omega_K^2 > 0$, where Ω_K is the angular frequency for a test mass (the Keplerian frequency). Thus the radial force balance equation reads

$$\rho g = \rho r \Omega^2 - \frac{d\Pi}{dr} - \frac{B_\phi^2}{4\pi r}. \quad (6)$$

To investigate the dynamical properties of the flow, we perturb the MHD Eqs. (1)-(3) by rewriting any physical variable f as $f + \delta f$ with $|\delta f| \ll |f|$. Since the unperturbed state is axisymmetric and steady, we consider all perturbation variables having the form $\delta f \propto e^{im\phi - i\omega t}$, with m being the azimuthal mode number and ω the wave frequency. Note that the background flow and magnetic field have no z -dependence and we assume that the perturbations also have no z -dependence. The resulting linearized perturbation equations contain the variables $\delta \mathbf{v}$, $\delta \rho$, δP , $\delta \Pi$ and $\delta \mathbf{B}$. For mathematical convenience, we define a new variable

$$\delta h = \frac{\delta \Pi}{\rho} = \frac{\delta P}{\rho} + \frac{\mathbf{B} \cdot \delta \mathbf{B}}{4\pi\rho}. \quad (7)$$

Moreover, using $\Delta \mathbf{v} = \delta \mathbf{v} + \boldsymbol{\xi} \cdot \nabla \mathbf{v} = d\boldsymbol{\xi}/dt = -i\omega \boldsymbol{\xi} + (\mathbf{v} \cdot \nabla) \boldsymbol{\xi}$, we find that the Eulerian perturbation $\delta \mathbf{v}$ is related to the Lagrangian displacement vector $\boldsymbol{\xi}$ by $\delta \mathbf{v} = -i\tilde{\omega} \boldsymbol{\xi} - r\Omega' \xi_r \hat{\phi}$, where prime denotes radial derivative and

$$\tilde{\omega} = \omega - m\Omega, \quad (8)$$

is the Doppler-shifted wave frequency. In the next two subsections, we will combine the perturbations equations into two first-order differential equations (ODEs) in terms of ξ_r and δh for the magnetosphere region and the disc region, respectively.

2.1 The magnetosphere

In the magnetosphere region ($r < r_{\text{in}}$), the flow is assumed to be incompressible and have uniform density (ρ is constant). For this particular magnetized fluid system, the detailed linearized perturbation equations have been given in Fu & Lai (2011b). Here we just display the final two ODEs for ξ_r and δh :

$$\frac{d\xi_r}{dr} = A_{11}\xi_r + A_{12}\delta h, \quad (9)$$

$$\frac{d\delta h}{dr} = A_{21}\xi_r + A_{22}\delta h, \quad (10)$$

where

$$A_{11} = -\frac{1}{r} \frac{\tilde{\omega}^2 - 2m\tilde{\omega}\Omega + m^2\omega_{A\phi}^2}{\tilde{\omega}^2 - m^2\omega_{A\phi}^2}, \quad (11)$$

$$A_{12} = \frac{m^2}{r^2}, \quad (12)$$

$$A_{21} = \tilde{\omega}^2 - m^2\omega_{A\phi}^2 - 2r\Omega \frac{d\Omega}{dr} + \left(2 \frac{d \ln B_\phi}{d \ln r} - 1\right) \omega_{A\phi}^2 - 4 \frac{(\tilde{\omega}\Omega + m\omega_{A\phi}^2)^2}{(\tilde{\omega}^2 - m^2\omega_{A\phi}^2)}, \quad (13)$$

$$A_{22} = \frac{2m}{r} \frac{\tilde{\omega}\Omega + m\omega_{A\phi}^2}{\tilde{\omega}^2 - m^2\omega_{A\phi}^2}, \quad (14)$$

and $\omega_{A\phi} \equiv v_{A\phi}/r = B_\phi/(r\sqrt{4\pi\rho})$ is the toroidal Alfvén frequency. Note that although we assume low plasma density for the magnetosphere, we still require that density is not too low in order to keep Alfvén speed far less than the speed of light. Otherwise, our original MHD equations break down (e.g., Lovelace, Romanova & Newman 2010). Also note that Eqs. (9) and (10) are the same as Eqs. (119) and (120) (derived for a purely toroidal magnetic field) of §83 in Chandrasekhar (1961). The vertical magnetic field B_z does not appear in our perturbation equations because we assumed $k_z = 0$, i.e., vertical field lines are not perturbed.

Defining $\sigma^2 = \tilde{\omega}^2 - m^2\omega_{A\phi}^2$, we can further combine Eqs. (9) and (10) into one single equation

$$\xi_r'' + \frac{d}{dr} \ln(r^3\sigma^2)\xi_r' + \frac{1-m^2}{r^2}\xi_r = 0. \quad (15)$$

Two special cases are of interest:

(i) For systems with $B_\phi = 0$, Eq. (15) reduces to

$$\xi_r'' + \left(\frac{3}{r} - \frac{2m\Omega'}{\tilde{\omega}}\right)\xi_r' + \frac{1-m^2}{r^2}\xi_r = 0, \quad (16)$$

or equivalently

$$W'' + \frac{W'}{r} - \frac{m^2}{r^2} \left[1 - \frac{r}{m\tilde{\omega}} \frac{d}{dr} \left(\frac{\kappa^2}{2\Omega}\right)\right] W = 0, \quad (17)$$

where $W = r\delta v_r$ and

$$\kappa = \left[\frac{2\Omega}{r} \frac{d}{dr}(r^2\Omega)\right]^{1/2} \quad (18)$$

is the radial epicyclic frequency. Note that Eq. (17) recovers Eq. (12) in Tsang & Lai (2009b). For either uniform rotation profile [$\Omega = \text{const}$, $\kappa = 2\Omega$, thus $(\kappa^2/2\Omega)' = 0$] or uniform angular momentum profile ($\Omega \propto r^{-2}$, thus $\kappa = 0$), it has the same simple solution

$$W \propto r^m \quad \text{or} \quad \delta v_r \propto r^{m-1}. \quad (19)$$

The corresponding solution for ξ_r is

$$\xi_r \propto r^{m-1} \quad \text{if} \quad \Omega = \text{const}; \quad \xi_r \propto \frac{r^{m-1}}{\omega - m\Omega(r)} \quad \text{if} \quad \Omega \propto r^{-2}. \quad (20)$$

(ii) In the special case of $\Omega = \text{const}$ and $B_\phi \propto r$ so that $\omega_{A\phi} \propto B_\phi/r\sqrt{\rho}$ is constant (note that we have assumed constant density in the magnetosphere), $[\ln(r^3\sigma^2)]'$ in Eq. (15) reduces to $[\ln(r^3\tilde{\omega}^2)]'$. Therefore magnetic fields in Eq. (15) (which enters through term σ^2) completely disappear and the equation is exactly the same as the one for $\Omega = \text{const}$ and $B_\phi = 0$. So the solutions for the magnetosphere region in this case are also $\xi_r \propto r^{m-1}$, $\delta h \propto r^m$ and the relation between these two wavefunctions can be obtained by substituting them back into Eqs. (9)-(10). Our calculations will focus on this particular magnetosphere setup.

2.2 The disc

In the disc region ($r > r_{\text{in}}$), we assume the flow is barotropic so that $\delta P = c_s^2 \delta \rho$ with $c_s = \sqrt{dP/d\rho}$ being the sound speed, which will be parametrized by a constant $\hat{c}_s \equiv c_s/(r\Omega)$ in our computation. For concreteness, we will also assume a power-law disc density profile $\rho \propto r^{-p}$ with p being a constant. For simplicity, we take the disc toroidal magnetic field to be uniformly distributed, i.e., $B_\phi = \text{const}$. From Eq. (6), we obtain the disc rotation profile as

$$\Omega(r) \simeq \frac{\Omega_K(r)}{\sqrt{1 + p\hat{c}_s^2}}. \quad (21)$$

In the above expression, we have ignored the effect of magnetic field as the disc field is supposed to be fairly weak in our model (see Fig. 1). The perturbation equations in component form can also be presented in the same form as Eqs. (9) and (10) with the detailed expressions of A_{11} , A_{12} , A_{21} and A_{22} given in Fu & Lai (2011a). For a non-magnetic disc, these equations reduce to

$$\frac{d\xi_r}{dr} = \left[-\frac{2m\Omega}{r\tilde{\omega}} - \frac{d\ln(r\rho)}{dr} \right] \xi_r + \left(\frac{m^2}{r^2\tilde{\omega}^2} - \frac{1}{c_s^2} \right) \delta h, \quad (22)$$

$$\frac{d\delta h}{dr} = (\tilde{\omega}^2 - \kappa^2)\xi_r + \frac{2m\Omega}{r\tilde{\omega}}\delta h. \quad (23)$$

2.3 The interface

In the equilibrium state, pressure balance at the interface reads

$$P_m + P_{bz} + P_{b\phi} = P_d, \quad (24)$$

where P_m , P_{bz} and $P_{b\phi}$ are the magnetosphere gas pressure, magnetic pressure of B_z and magnetic pressure of B_ϕ just inside the interface, respectively, while P_d is the disc total pressure just outside the interface. This equality imposes an upper limit on the strength of the magnetosphere toroidal B field, $P_{b\phi}/P_d < 1$. Defining $b = (\omega_{A\phi})|_{r_{\text{in}}}/\Omega_d$ and $\mu = (\rho_d - \rho_m)/(\rho_d + \rho_m)$, where Ω_d is the disc rotation rate at the interface, ρ_m and ρ_d are the fluid densities of the magnetosphere and the disc at the interface, respectively, then the above inequality becomes

$$\frac{P_{b\phi}}{P_d} \simeq \frac{(1-\mu)b^2}{(1+\mu)2\hat{c}_s^2} \quad (25)$$

Note that in the magnetosphere, magnetic pressure dominates over gas pressure ($P_{bz} + P_{b\phi} \gg P_m$). So $P_{b\phi}/P_d \simeq P_{b\phi}/(P_{b\phi} + P_{bz})$ approximately characterizes the relative strength of the toroidal field compared to the vertical field.

In the perturbed state, we demand that both the radial Lagrangian displacement ξ_r and the Lagrangian perturbation of total pressure $\Delta\Pi = \delta\Pi + \xi_r\Pi'$ be continuous across the interface. The latter of these requirements yields

$$\rho_m [\delta h + \xi_r r (\Omega^2 - \Omega_K^2 - \omega_{A\phi}^2)]_{r_{\text{in}-}} = \rho_d [\delta h - \xi_r r p \hat{c}_s^2 \Omega^2]_{r_{\text{in}+}}. \quad (26)$$

In the magnetosphere, we have the analytical solutions for δh ($\propto r^m$) and ξ_r ($\propto r^{m-1}$) (see Sec. 2.1), which are related via

$$\delta h = \frac{r}{m} [\tilde{\omega}^2 + 2\tilde{\omega}\Omega + m(2-m)\omega_{A\phi}^2] \xi_r. \quad (27)$$

We substitute this relation into the left hand side of Eq. (26) and consolidate it with another requirement (continuity of ξ_r) to obtain the matching condition across the interface

$$\frac{(\omega - m\Omega_m)[\omega - (m-2)\Omega_m]}{m} + \Omega_m^2 = \frac{1+\mu}{(1-\mu)r_{\text{in}}} \frac{\delta h}{\xi_r} + \left[1 - \frac{2\mu p \hat{c}_s^2}{1-\mu} + (m-1)b^2 \right] \Omega_d^2, \quad (28)$$

where δh and ξ_r are disc solutions at the interface, Ω_m and Ω_d are the rotation rates of the magnetosphere and the disc at the interface, respectively. In the case of $B_\phi = 0$ in the magnetosphere, this matching condition reduces to Eq. (22) in Tsang & Lai (2009b). Note that Eq. (28) has no explicit dependence on the disc magnetic field. This has to do with the fact that we chose an uniformly distributed disc B field.

3 INTERFACE MODES: NEWTONIAN POTENTIAL

Li & Narayan (2004) and Tsang & Lai (2009b), who considered incompressible and compressible discs respectively, have shown that interface modes of magnetosphere-disc boundary can be subject to Rayleigh-Taylor and/or Kelvin-Helmholtz instabilities, depending on the density contrast and velocity shear across the interface. In order to investigate the effects of magnetosphere toroidal magnetic fields on these instabilities, in this section we assume the disc region to be magnetic-field free and employ the standard shooting method (Press et al. 1992) to solve Eqs. (22)-(23) using the matching condition Eq. (28) as the inner boundary condition at r_{in} and outgoing wave condition (Tsang & Lai 2009b) at the outer boundary of the disc (r_{out}). The complex mode frequency ω can then be determined as an eigenvalue of the system. Note that in general we also need to apply shooting method in the magnetosphere region (see Appendix A), but for the specific magnetic field profile (and uniform rotation) of the magnetosphere we chose in this study, the perturbation equations in the magnetosphere have simple analytic solutions (see §2.2) and the effect of magnetosphere on the interface modes is embodied by the interface matching condition (i.e, inner boundary condition for disc perturbation equations).

In our computation, we use $p = 1.5$, $\hat{c}_s = 0.15$, and put the outer boundary at $r_{\text{out}} = 2.85r_{\text{in}}$. We vary the strength of magnetosphere toroidal magnetic field b (therefore $P_{b\phi}/P_d$; Eq. [25]) for different sets of $(\Omega_m/\Omega_d, \rho_m/\rho_d)$ to see how the

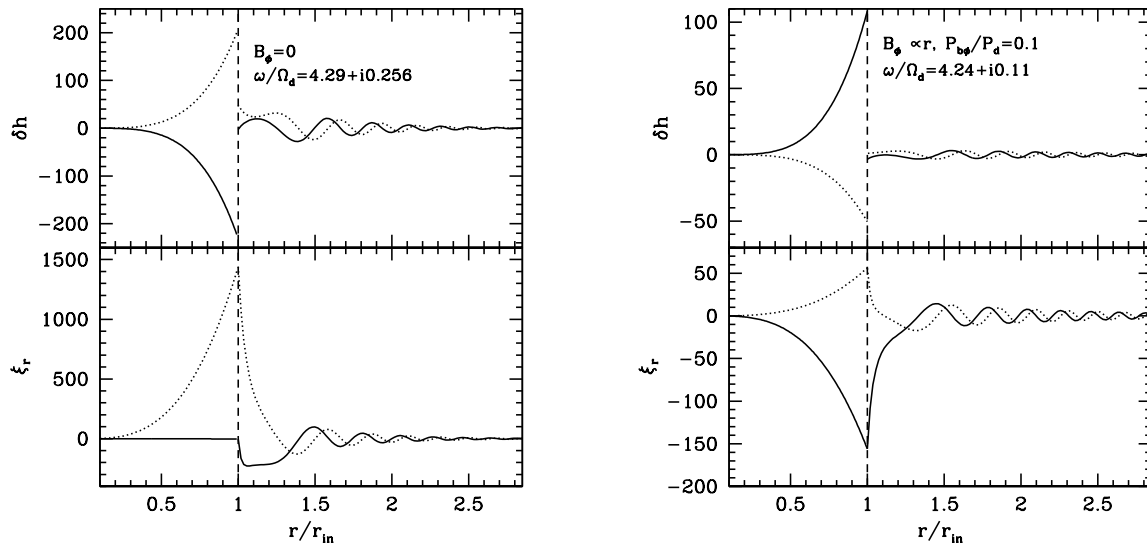


Figure 2. The wavefunctions for the unstable interface mode with $m = 4$, $\rho_m/\rho_d = 1/99$, $\Omega_m/\Omega_d = 1$ in a magnetosphere-disc system without (left) and with (right) magnetosphere toroidal magnetic field, respectively. The vertical long-dashed lines mark the position of the interface which separates magnetosphere region and disc region. The solid and dotted lines represent the real and imaginary parts of the wavefunctions, respectively.

eigenvalue ω will be modified. Throughout this section, we use Newtonian potential $\Phi = -GM/r$, so that the Keplerian frequency is $\Omega_K = (GM/r^3)^{1/2}$, and the epicyclic frequency κ equals Ω .

3.1 Numerical solutions

Fig. 2 shows two example wavefunctions for the unstable interface mode. The left panel depicts the case with no toroidal magnetic field in the magnetosphere (but keep in mind that there is always finite vertical B field) while in the right panel the magnetosphere has a non-zero B_ϕ . Since there is no velocity shear across the boundary in both cases ($\Omega_m/\Omega_d = 1$), the instability is of Rayleigh-Taylor type. We see that the addition of toroidal field has a small effect on the eigenfunction. However, as the numbers in the figure indicate, the growth rate of the unstable mode is reduced by more than 50% (from $0.256\Omega_d$ to $0.11\Omega_d$) even though the the toroidal magnetic field pressure is only 10% of the disc gas pressure (both evaluated at the interface), i.e. even though the toroidal field is much weaker than vertical field in the magnetosphere.

The suppressing effect of toroidal magnetic field on the instability can be more easily seen in Fig. 3, where we plot the real and imaginary parts of the eigen-frequencies for the interface mode as a function of B_ϕ . We consider four different sets of $(\Omega_m/\Omega_d, \rho_m/\rho_d)$ such that the panels in the same row have the same velocity shear but different density contrast while the panels in the same column have the same density contrast but different velocity shear. The modes in the top two panels are subject to Rayleigh-Taylor type instability as there are no velocity shear at the interface. The bottom two panels, however, have non-zero velocity shear, thus are subject to instabilities of both Rayleigh-Taylor and Kelvin-Helmholtz types. In all cases, we observe that the inclusion of toroidal magnetic fields can significantly diminish the growth rate of the unstable modes, even completely kill the instability. The critical B_ϕ for absolute shut-down of unstable modes depends on the detailed interface parameters (sound speed in the disc, velocity shear, density contrast, etc.). In the case with the most unstable modes (bottom-right panel) that we have calculated, the required $P_{b\phi}/P_d$ to fully turn off the mode growth is close to one. This means that the toroidal magnetic field needs to dominate over the vertical field in the magnetosphere (remember that $P_{b\phi}/P_d \simeq P_{b\phi}/(P_{b\phi} + P_{bz})$). The mode frequencies (real part of ω), on the other hand, are barely affected by B_ϕ (at least when the growth rate is not very small). By comparing panels in the same column, we see that increasing velocity shear at the interface leads to larger growth rates, which is not surprising as more velocity shear means more free energy that the system can tap on to drive the instability. Comparing panels in the same row reveals an interesting features. We found that larger density contrasts leads to smaller growth rates, which apparently contradicts the standard Rayleigh-Taylor instability result. In particular, the $m = 1$ mode is totally stable when $\rho_m/\rho_d = 1/99$ while becomes unstable when $\rho_m/\rho_d = 1/9$ and B_ϕ does not affect the $m = 1$ mode at all. Comparing different lines in each individual panel shows that modes with larger m generally have larger growth rates, but they are also more easily stabilized by the toroidal field.

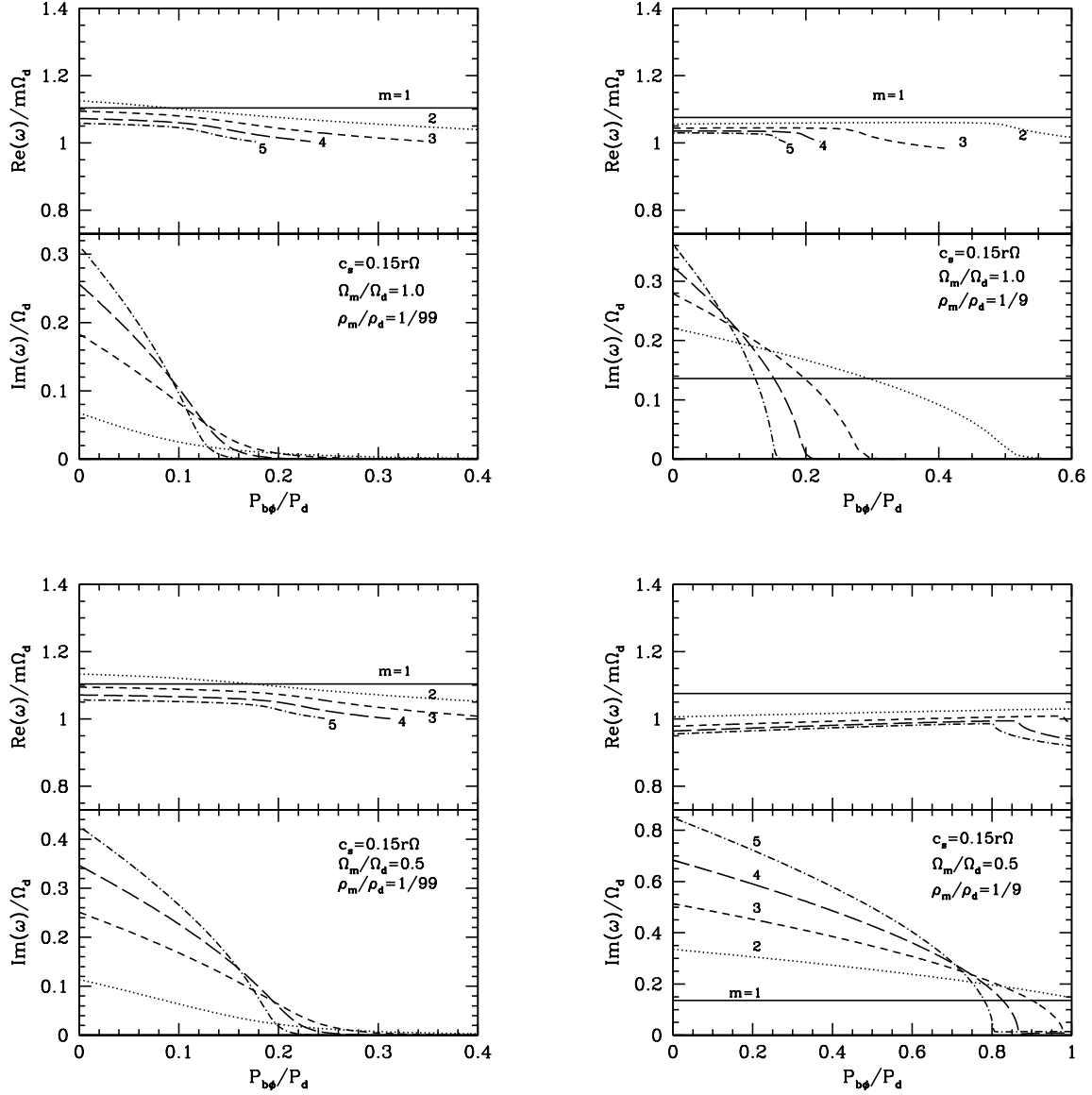


Figure 3. Real and imaginary parts of the wave frequencies (in units of Ω_d , the disc rotation rate at the interface) for unstable interface modes as a function of magnetosphere toroidal magnetic field strength. The top and bottom panels are for the cases without and with velocity shear at the interface, respectively, while the left and right panels depict models with the magnetosphere to disc density ratio being 1/99 and 1/9, respectively. Different line types are associated with different values of m , with the solid lines for $m = 1$, dotted lines for $m = 2$, short-dashed lines for $m = 3$, long-dashed lines for $m = 4$, and dot-dashed lines for $m = 5$.

3.2 Discussion of results

The zero effect of B_ϕ on the $m = 1$ mode (whether it is stable or unstable) can be easily understood by looking at the matching condition Eq. (28). This equation (i.e., inner boundary condition for disc equations) is the only place that B_ϕ affects the eigenvalue problem, and the magnetic effect comes in via the last term on the right hand side of the equation $[(m-1)b^2\Omega_d^2]$. When $m = 1$, this term vanishes so that the equation is the same as in the case with zero B_ϕ .

To explain the other features observed in Fig. 3, we carry out a local analysis of the effects of magnetic fields on Rayleigh-Taylor/Kelvin-Helmholtz instability in a plane-parallel flow (see Appendix B). From the last term in the final expression of wave frequency (Eq. [B1]), we see that magnetic tension ($\mathbf{k} \cdot \mathbf{B}$) provides a suppressing force against Rayleigh-Taylor/Kelvin-Helmholtz instability of a two-layered fluid system. This is because extra work needs to be done in order to increase the boundary layer deformation (i.e., growing perturbation). Our cylindrical magnetosphere-disc model resembles the simple parallel two-layered flow in that our wavenumber in azimuthal direction m/r acts like k in the x direction and our B_ϕ also

lies along the direction of the wave vector. Thus, the same stabilizing mechanism also applies in our system, i.e., the tension force of the toroidal magnetic field suppresses the magnetosphere-disc interface instability.

Qualitatively, the growth rate of interface modes in our system is determined by combined effects of four factors: density contrast (ρ_m/ρ_d), velocity shear across the interface (Ω_m/Ω_d), degree of differential rotation in the disc, and toroidal field of the magnetosphere. The first two tend to enhance instability, while the latter two tend to suppress instability. In different limiting cases, approximate analytic expressions for the mode growth rate can be derived: Li & Narayan (2004) considered a case where the disc is incompressible with constant density and came up with their Eq. (45), while Tsang & Lai (2009b) studied a compressible disc whose density is much larger than the magnetosphere density, and summarized the results in their Eqs. (26) and (28). Although for the generic conditions studied in this paper, an analytical expression cannot be rigorously derived, we can write the mode growth rate schematically as follows:

$$\omega_i \sim \sqrt{\omega_{\text{RT}}^2 + \omega_{\text{KH}}^2 - \omega_{\text{vort}}^2 - \omega_b^2} \quad (29)$$

with

$$\omega_{\text{RT}}^2 \simeq 2(1 + \mu)m\Omega_{\text{eff},d}^2 - 2(1 - \mu)m\Omega_{\text{eff},m}^2, \quad (30)$$

$$\omega_{\text{KH}}^2 \simeq (1 - \mu^2)m^2(\Omega_d - \Omega_m)^2 + 2(1 - \mu^2)m(\Omega_d - \Omega_m)(\zeta_d - \zeta_m), \quad (31)$$

$$\omega_{\text{vort}}^2 \simeq (\zeta_d - \zeta_m)^2 + 2\mu(\zeta_d^2 - \zeta_m^2) + \mu^2(\zeta_d + \zeta_m)^2, \quad (32)$$

$$\omega_b^2 \simeq \frac{m^2 B_\phi^2}{4\pi r^2(\rho_d + \rho_m)} \simeq (1 - \mu)m^2\omega_{A\phi}^2/2, \quad (33)$$

where $r\Omega_{\text{eff}}^2 = d\Phi/dr - r\Omega^2$ is the effective gravitational acceleration, $\zeta = \kappa^2/(2\Omega)$ is the fluid vorticity and as before the subscripts d and m denote disc and magnetosphere, respectively. Several features can be noted in Eq. (29):

(i) The first two terms under the square root are the Rayleigh-Taylor and Kelvin-Helmholtz types of destabilizing factors while the last two terms characterize the stabilizing effects due to flow vorticity and toroidal magnetic field in the magnetosphere, respectively. The suppressing effect of finite fluid vorticity has been discussed in both Li & Narayan (2004) and Tsang & Lai (2009b). We see that the various terms have different dependences on the density contrast μ . As μ increases ($\mu = 0$ when $\rho_m/\rho_d = 1$, and $\mu = 1$ when $\rho_m/\rho_d = 0$), ω_{RT}^2 increases, making the system more Rayleigh-Taylor unstable; at the same time, ω_{KH}^2 decreases, making the system less Kelvin-Helmholtz unstable. In addition, ω_{vort}^2 also becomes larger, leading to stronger suppressing effect. This explains why in Fig. 3, the mode with $\rho_m/\rho_d = 1/99$ is less unstable than the one with $\rho_m/\rho_d = 1/9$.

(ii) Since $\Omega_{\text{eff},d}^2 = (1/r)(d\Phi/dr) - \Omega^2 = -(c_s^2/\rho)(d\rho/dr)$, when c_s is too small (i.e., small effective gravity in the disc), the destabilizing terms would not be able to compete with the stabilizing terms, resulting in a stable system. Thus, a sufficiently high disc sound speed is needed to attain the interface instability (see Tsang & Lai 2009b).

(iii) When there is no B_ϕ , we see that ω_{RT}^2 and ω_{KH}^2 both depend on m while ω_{vort}^2 does not. Thus, modes with higher m tend to be more unstable, as shown in Fig. 3 (the $P_{b\phi}/P_d = 0$ case; see also Li & Narayan 2004 and Tsang & Lai 2009b). The $m = 1$ mode would be even less unstable if the density contrast is too big [see (i) above]. This explains why in Fig. 3 the $m = 1$ mode with $\rho_m/\rho_d = 1/99$ is stable while the one with $\rho_m/\rho_d = 1/9$ is unstable.

(iv) When $B_\phi \neq 0$, besides ω_b^2 , the magnetic field strength also appears in ω_{RT}^2 where $\Omega_{\text{eff},m}^2$ contains a term that is proportional to $-B_\phi^2/4\pi\rho_m r^2$ (note the minus sign). This shows that the toroidal field in the magnetosphere plays two different roles in determining the stability of system. On the one hand, the magnetic tension resists perturbation growth, thus suppressing any instability; on the other hand, the magnetic force increases the effective gravity (pointing towards the center) of the background flow, thus promoting Rayleigh-Taylor type instability. The former effect is proportional to m while the latter to m^2 . Hence, in general the suppressing effect is more important. This is consistent with the fact that in Fig. 3 the growth rates of modes with higher m decrease more rapidly as B_ϕ increases. As noted above, B_ϕ does not affect the $m = 1$ mode because the last term in Eq. (28) vanishes for $m = 1$. Now we have a better understanding of what this means physically: For the $m = 1$ mode, the aforementioned two opposing effects associated with B_ϕ happen to cancel each other. This exact cancellation, however, cannot be captured by the approximate expression Eq. (29).

Overall, we see that Eq. (29), though schematic, is quite useful in explaining most of the numerical results of this section. Note that various flow parameters, such as the density contrast μ , azimuthal mode number m , toroidal magnetic field B_ϕ and disc vorticity ζ_d , appear in more than one of the four terms in this equation. Thus, they are associated with both the stabilizing and destabilizing effects. The only exception is perhaps the velocity shear at the interface, which always facilitates the interface instability.

Finally, we note that the interface instability associated with magnetosphere-disc boundary studied in this paper is qualitatively different from those of Lubow & Spruit (1995) and Spruit, Stehle & Papaloizou (1995), who carried out local analysis of a thin rotating disc threaded by a large-scale poloidal field. Lovelace, Romanova & Newman (2010) considered similar interface instability as in our paper, but they focused on small-scale modes and included only vertical field in the magnetosphere.

4 INTERFACE MODES AND DISCOSEISMIC MODES: PSEUDO-NEWTONIAN POTENTIAL

In this section, we consider how the global oscillation modes in our disc-magnetosphere system (Fig. 1) are modified by general relativistic (GR) effects. In particular, GR changes the disc rotation profile $\Omega_K(r)$ and makes the radial epicyclic frequency $\kappa(r)$ a non-monotonic function of r : As r decreases, κ first increases, attains a maximum value and then falls to zero at the Innermost Stable Circular Orbit (ISCO), $r_{\text{ISCO}} = 6GM/c^2$ (for a non-spinning compact object). If the inner disc boundary is close to r_{ISCO} , then this non-monotonic κ profile can have two consequences: (1) It significantly reduces disc vorticity ($\kappa^2/2\Omega$) near the inner disc boundary, therefore helps the unstable interface modes grow as there are less disc vorticity suppressing effects (see the discussion in Section 3.2; see also Tsang & Lai 2009b); (2) It could lead to a vortensity ($\kappa^2/2\Omega\rho$ a.k.a potential vorticity) profile that has positive gradient in the inner disc region. As found in our previous studies (Tsang & Lai 2008; Lai & Tsang 2009; Fu & Lai 2011a), positive vortensity gradient renders the disc inertial-acoustic modes (p-modes) unstable. In Section 3, we chose a density profile $\rho \propto r^{-3/2}$ so that the vortensity profile (with the Newtonian potential) is completely flat, and thus we only found unstable (overstable) interface modes. In this section, with the GR effect included, both the interface modes and disc p-modes can be unstable and they co-exist in our disc-magnetosphere system. The main goal of this section is then to study these two modes and the effects of the magnetosphere toroidal B field, disc toroidal B field and inner disc boundary location.

We employ the pseudo-Newtonian potential (Paczynski & Wiita 1980) to mimic the GR effect:

$$\Phi = -\frac{GM}{r-r_S}, \quad (34)$$

where $r_S = 2GM/c^2$ is the Schwarzschild radius. The corresponding Keplerian rotation frequency and epicyclic frequency are

$$\Omega_K = \sqrt{\frac{GM}{r} \frac{1}{r-r_S}}, \quad (35)$$

$$\kappa = \Omega \sqrt{\frac{r-3r_S}{r-r_S}}. \quad (36)$$

Except for Section 4.3, we will take the magnetosphere-disc interface to be located at the ISCO, $r_{\text{in}} = r_{\text{ISCO}} = 3r_S$.

4.1 Non-magnetic discs

We first consider the case where the disc outside the magnetosphere is non-magnetic. We solve the same equations and use the same interface boundary condition as in Section 3 except that we replace the Newtonian potential with Pseudo-Newtonian potential.

Figure 4 shows the complex eigenfrequencies of disc inertial-acoustic modes and interface modes as a function of the dimensionless magnetosphere toroidal field strength $P_{b\phi}/P_d$. The other parameters are indicated in the figure. As noted above, because of the GR effect, the disc vortensity profile has a positive slope near the ISCO (see Fig. 5). The disc inertial-acoustic mode (p-mode) of lowest radial order (for a given m) has $\text{Re}(\omega) < m\Omega_d$, and the corotation resonance lies in the disc (see the right panels of Fig. 6 for an example). Corotational wave absorption then makes these modes unstable. We see from Fig. 4 that as long as there is a magnetosphere to serve as an inner boundary condition for the disc mode, the mode frequency and growth rate depend rather weakly on $P_{b\phi}/P_d$.

The interface mode is also strongly influenced by the the GR effect. Comparing the right panels of Fig. 4 with the bottom-left panel of Fig. 3, we see that for $P_{b\phi} = 0$, the mode growth rate (for a given m) is larger when the GR effect is included. Again, this is because in GR, the disc vorticity is smaller near the ISCO, leading to less rotational suppression of the RT instability (see Section 3.2). As $P_{b\phi}/P_d$ increases, the interface mode growth rate first decreases (just as in the Newtonian case) due to magnetic tension, then starts to increase beyond certain critical value of $P_{b\phi}/P_d$ (for a given m). This behaviour arises from the effect of corotation resonance (see Fig. 5): For small $P_{b\phi}/P_d$, the interface mode has $\text{Re}(\omega) > m\Omega_d$, thus no corotation resonance exists in the flow; as $P_{b\phi}/P_d$ becomes larger, the mode frequency drops below $m\Omega_d$, and corotation resonance comes into play, which overwhelms the suppression effect of the magnetic tension (see the left and middle panels of Fig. 6 for two examples of mode wavefunctions). The growth rate of such interface mode (labelled as Type II in Fig. 5) is much larger than the corresponding disc p-mode because the corotation resonance lies much closer to r_{in} for the interface mode than for the p-mode – this gives rise to much stronger wave absorption at the corotation resonance.

4.2 Magnetic discs

Now we consider the case in which the disc outside the magnetosphere has a finite toroidal magnetic field. For simplicity, we take the limit that the density in the magnetosphere ρ_m goes to zero. In this case, the interface boundary condition Eq. (28) reduces to $\Delta\Pi = 0$, i.e., the Lagrangian perturbation of total disc pressure equals zero at r_{in} . With this boundary condition, the setup is the same as in Fu & Lai (2011a) and we only need to consider the dynamical equations for the disc.

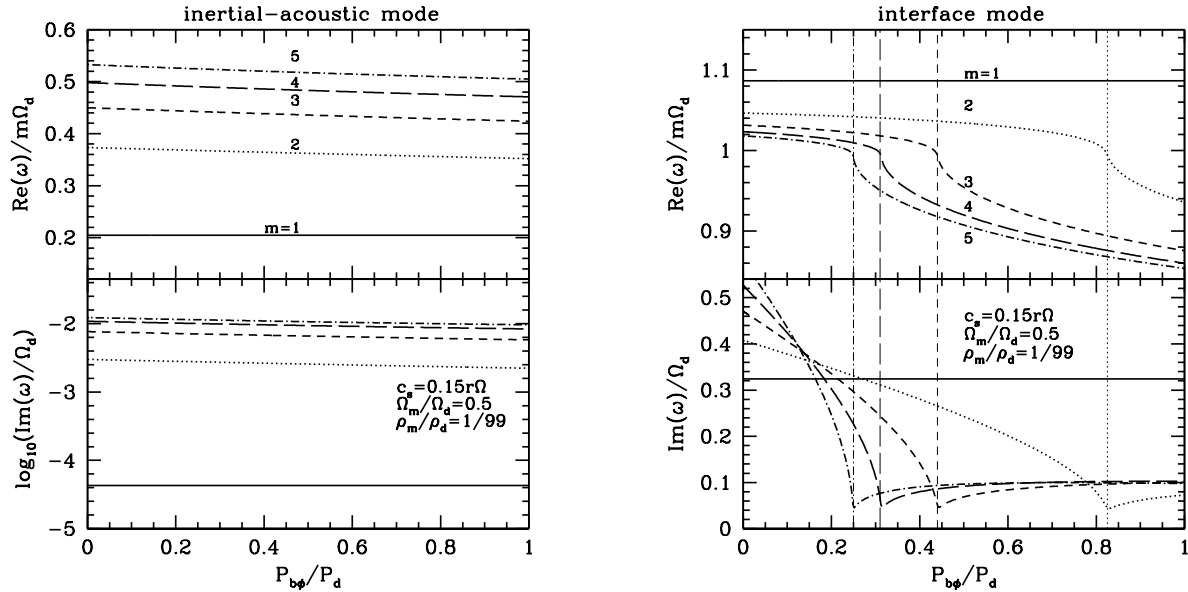


Figure 4. Real and imaginary parts of the wave frequencies (in units of Ω_d , the disc rotation rate at r_{in}) for unstable inertial-acoustic disc modes (left panels) and unstable interface modes (right panels) as a function of the magnetosphere toroidal field strength. Different line types represent different azimuthal mode number m . The sound speed profile, density contrast and velocity shear across the interface are the same as in the bottom-left panel of Fig. 3. The only difference from Fig. 3 is that GR effect (using pseudo-Newtonian potential) is included in the disc rotation profile, which renders both types of modes unstable. On the right panels, the vertical lines (for $m = 2$ and 3) mark the point when corotation resonance moves into the flow (see Fig. 5).

Again, two types of oscillation modes exist in our system (see Fig. 7): the disc inertial-acoustic modes and interface modes. The effect of the disc magnetic field on the inertial-acoustic modes has already been studied in detail by Fu & Lai (2011a). We see from the left panels of Fig. 7 that the mode frequency is only slightly modified by the disc B_ϕ , but the growth rate is reduced so that the mode become stable even for modest (sub-thermal) disc toroidal fields.

The interface mode (the right panels of Fig. 7) was not considered by Fu & Lai (2011a). We see that as the disc magnetic field increases, the mode frequency varies modestly (about 10%) for a wide range of B_ϕ , but the growth rate changes more significantly. The dependence of the growth rate as a function of disc B_ϕ can be understood as follows: (i) For $B_\phi = 0$, RT instability drives the mode growth; (ii) As B_ϕ increases, the magnetic tension tends to suppress the growth; (iii) As B_ϕ increases, the real mode frequency decreases. When B_ϕ exceeds some critical value, corotation resonance appears in the flow (disc), and wave absorption at corotation then enhances the growth rate. But as B_ϕ increases further, the corotation radius lies at a larger distance from r_{in} , thus the corotational effect becomes less important (because of the large evanescent zone separating r_{in} and the corotation radius) and the mode growth rate decreases again also because of magnetic tension.

Concerning (iii) above, as noted in Fu & Lai (2011a), in the presence of the disc toroidal magnetic field, the corotation resonance (where $\tilde{\omega} = 0$) is split into the inner/outer magnetic resonances, where

$$\tilde{\omega} = \pm m\omega_{A\phi}, \quad (37)$$

where $\omega_{A\phi} = v_{A\phi}/r = B_\phi/(r\sqrt{4\pi\rho})$ is the toroidal Alfvén frequency of the disc. When these magnetic resonances exist in the flow (disc), wave absorption comes into play in the mode growth. Note that the signs of wave absorption at the two magnetic resonances are different. As $\text{Re}(\omega)$ decreases (with increasing B_ϕ), the outer magnetic resonance (where $\tilde{\omega} = m\omega_{A\phi}$) first enters the flow, causing the mode growth rate to increase. When the inner magnetic resonance (where $\tilde{\omega} = -m\omega_{A\phi}$) enters the flow, the wave absorptions at the two magnetic resonances partially cancel, and the mode growth rate starts to decrease again (see the right panels of Fig. 7). In this case, the term “corotation resonance” simply refers to the combined effect of two magnetic resonances.

4.3 Effects of different inner disc radii

Here we consider the same setup as in Sections 4.1-4.2 except that the inner disc boundary lies outside the ISCO. The motivation for considering $r_{\text{in}} > r_{\text{ISCO}}$ is that in real accreting NS systems, the magnetosphere radius may well be outside the ISCO (e.g., in accreting millisecond X-ray pulsars with surface magnetic field of 10^{8-9} G, the Alfvén radius is about 1.5-2

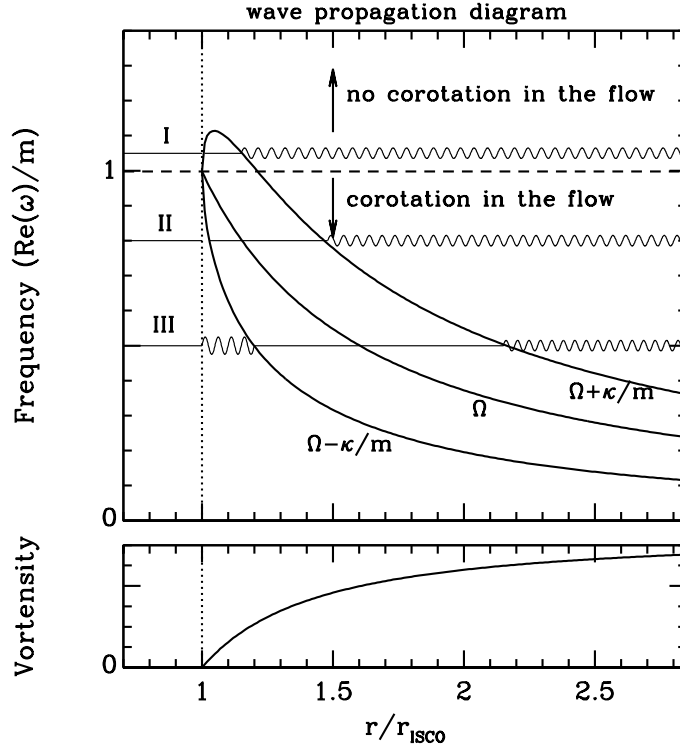


Figure 5. Wave propagation diagram (upper panel) for both interface modes and disc inertial-acoustic modes accompanied by the disc vortensity profile (lower panel). In the upper panel, the three thick solid curves depict the disc rotation profile Ω and $\Omega \pm \kappa/m$, where m is the azimuthal mode number and κ is the radial epicyclic frequency. Note that since $\kappa(r_{\text{ISCO}}) = 0$ these three curves join each other at the Innermost Stable Circular Orbit (which is also the disc inner boundary r_{in} in our setup of Sections 4.1 & 4.2). The dashed horizontal line marks the point when the corotation radius [where $\text{Re}(\omega)/m = \Omega$] happens to be exactly at the inner disc boundary. For modes with $\text{Re}(\omega)/m$ above this line, there is no corotation in the flow; for any modes with $\text{Re}(\omega)/m$ below this line, the corotation exists in the flow ($r_c > r_{\text{in}}$). Three types of wave modes (labeled as I, II and III) are shown in this diagram where the horizontal solid lines indicate the evanescent zones and the wavy curves denote the wave propagation zones. Note that for both Type I and II waves, there is also a tiny wave zone (hardly visible in the figure) in the disc region just outside the ISCO. Type I and II waves are both interface modes while type III waves are disc inertial-acoustic modes. Note that the magnetosphere region ($r < r_{\text{ISCO}}$) and the region between the inner and outer Lindblad resonances [where $\text{Re}(\omega)/m = \Omega \pm \kappa/m$] are wave evanescent zones.

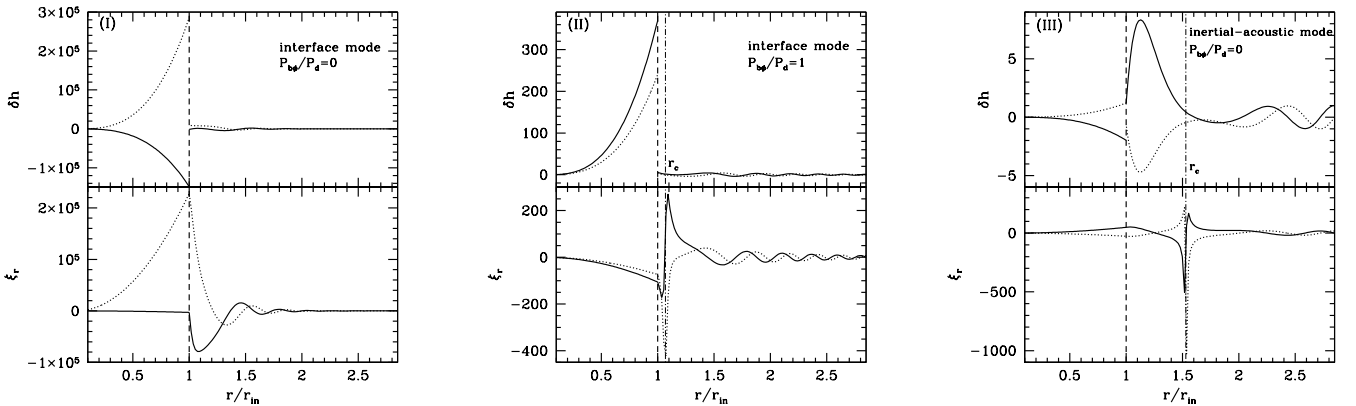


Figure 6. Wave functions for the three types of wave modes depicted in Fig. 5: the interface mode with no corotation resonance in the flow (Type I, left panels), interface mode with corotation resonance in the flow (Type II, middle panels) and disc inertial-acoustic mode (Type III, right panels). The azimuthal mode number is $m = 3$ and all other parameters are the same in Fig. 4. The solid and dotted lines show the real and imaginary parts, respectively. In the middle and right panels, the vertical dot-dashed lines represent the location of corotation resonance.

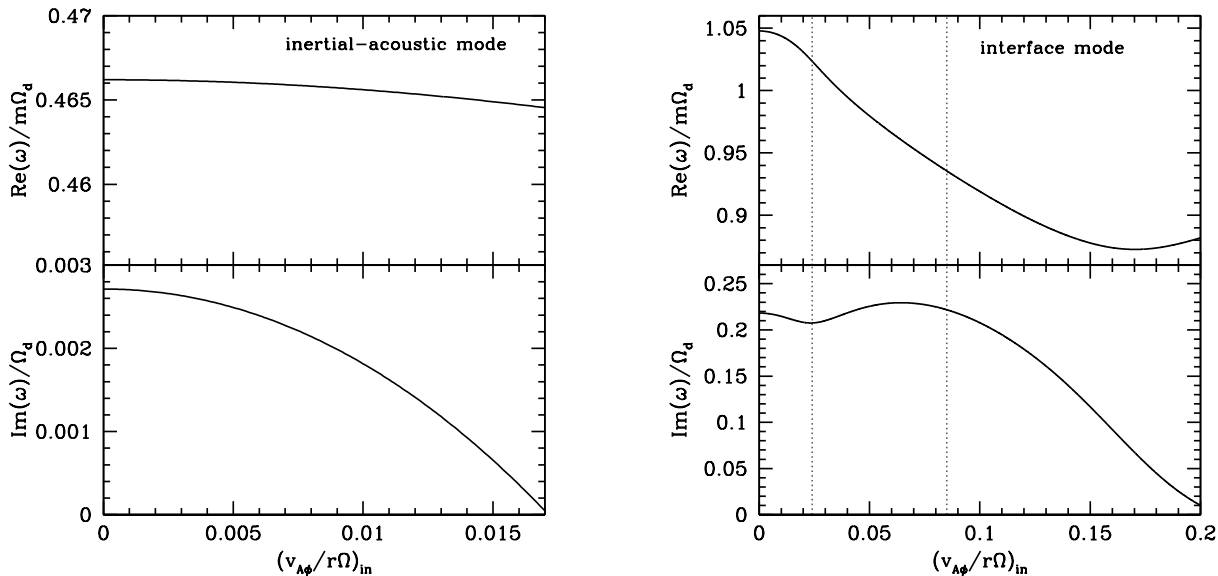


Figure 7. Real and imaginary parts of the wave frequencies (in units of Ω_d , the disc rotation rate at r_{in}) for unstable inertial-acoustic disc modes (left panels) and unstable interface modes (right panels) as a function of the disc toroidal field strength. The x -axis specifies the ratio of the Alfvén velocity to disc rotation velocity at the inner boundary r_{in} . The magnetosphere density is set to zero. The disc parameters are $r_{\text{in}} = r_{\text{ISCO}}$, $m = 2$, $c_s = 0.1r\Omega$ and $\rho \propto r^{-1}$. For the interface mode (right panels), the two dotted vertical lines from left to right mark the entering of the outer magnetic resonance and inner magnetic resonance into the flow, respectively.

stellar radii). Also, in the “transitional state” (when HFQPOs are observed) of BH X-ray binaries, the thin thermal disc may be truncated at a radius slightly larger than the ISCO (e.g., Done et al. 2007; Oda et al. 2010).

As in Section 4.2, we assume that the magnetosphere has a negligible density. Figure 8 shows an example (for a non-magnetic disc) of how the (complex) mode frequencies depend on r_{in} . When expressed in units of Ω_d , the real frequencies of both interface and inertial-acoustic modes are only modestly affected by $r_{\text{in}}/r_{\text{ISCO}}$, but the growth rates decrease rapidly with increasing $r_{\text{in}}/r_{\text{ISCO}}$. For the inertial-acoustic mode, this arises from the reduced vortensity slope at distances further away from the ISCO, which results in smaller wave absorption at corotation. For the interface mode, the larger vorticity just beyond r_{in} leads to a stronger rotational suppression of the RT instability, thus a smaller mode growth rate.

Figure 9 shows how the complex frequency of the interface mode depends on the disc magnetic field B_ϕ when the inner disc radius is set to $1.5r_{\text{ISCO}}$. The behaviour of the mode growth rate as a function of $(v_{A\phi}/r\Omega)_{\text{in}}$ is similar to the right panels of Fig. 7. Here, the mode growth rate is small when $B_\phi = 0$. So when the outer magnetic resonance enters the flow, wave absorption dramatically increases the mode growth rate.

5 DISCUSSION AND CONCLUSION

In this paper we have studied the non-axisymmetric MHD modes and instabilities in a 2D model of magnetosphere-disc systems (see Fig. 1), as may be realized in accreting neutron star or black-hole X-ray binaries (see Section 1). We have examined various physical effects and parameters that can influence the global modes in the system, including the density and magnetic field of the magnetosphere, the velocity contrast across the magnetosphere-disc interface, the rotation profile (Newtonian vs GR), the temperature and magnetic field of the disc. We restrict to modes that do not have vertical structure, but otherwise our calculations include all possible instabilities and global oscillations associated with the interface and the disc. We highlight several key findings and implications of this paper below.

5.1 Interface instabilities in a rotating, magnetized system

This paper includes a comprehensive study of the large-scale Rayleigh-Taylor (RT) and Kelvin-Helmholtz (KH) instabilities associated with the interface of a rotating, magnetized system. RT and KH instabilities have been studied intensively in plane-parallel flows through both theoretical analysis and laboratory experiments (e.g. Chandrasekhar 1961; Drazin & Reid 1981), and have found applications in various astrophysical and space environments. But few papers have focused on rotating systems (e.g., Spruit et al. 1995; Lovelace et al. 2009, 2010). Our study generalizes previous works by Li & Narayan (2004)

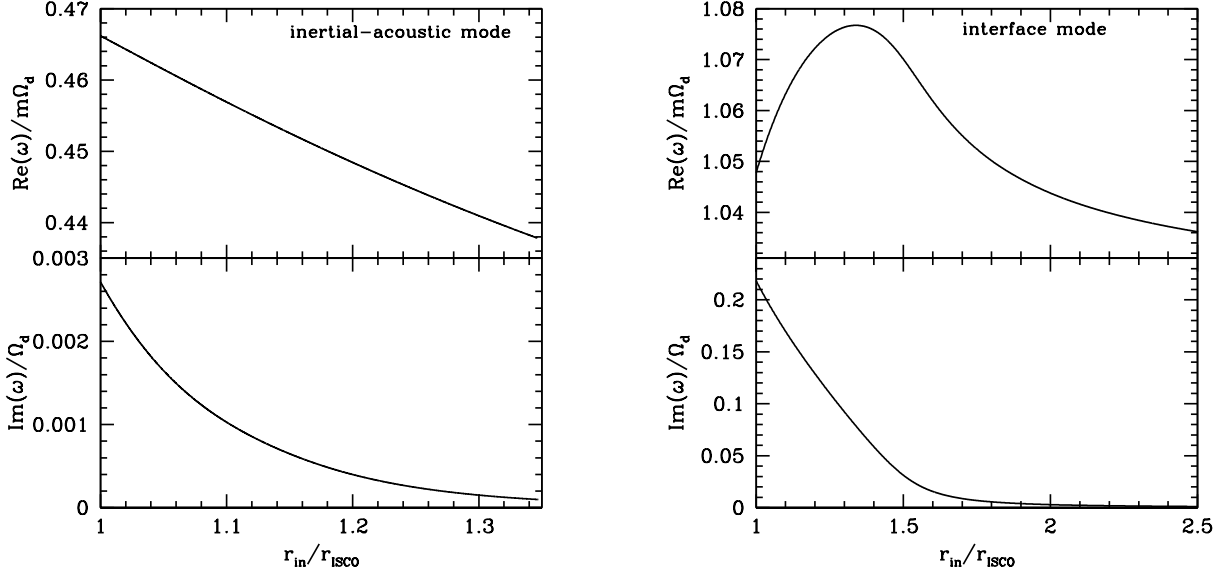


Figure 8. The real and imaginary parts of the wave frequencies (in units of Ω_d , the disc rotation rate at r_{in}) for unstable inertial-acoustic modes (left panels) and unstable interface modes (right panels) as a function of the inner disc radius r_{in} (in units of r_{ISCO}). The magnetosphere inside r_{in} has zero density and the disc toroidal magnetic field is set to zero. The other disc parameters are $m = 2$, $c_s = 0.1r\Omega$ and $\rho \propto r^{-1}$.

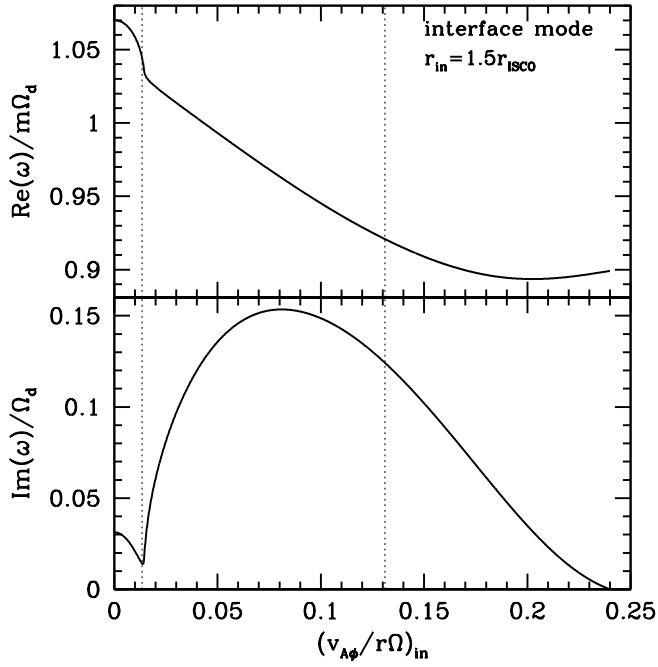


Figure 9. Real and imaginary parts of the wave frequencies (in units of Ω_d , the disc rotation rate at r_{in}) for unstable interface modes as a function of the disc toroidal field strength, with the inner disc boundary located at $r_{\text{in}} = 1.5r_{\text{ISCO}}$. The x -axis specifies the ratio of the Alfvén velocity to disc rotation velocity at r_{in} . The magnetosphere density is set to zero. The disc parameters are $r_{\text{in}} = r_{\text{ISCO}}$, $m = 2$, $c_s = 0.1r\Omega$ and $\rho \propto r^{-1}$. The two dotted vertical lines from left to right mark the entering of outer magnetic resonance and inner magnetic resonance into the flow, respectively.

and Tsang & Lai (2009b) by considering compressible fluid, magnetic field and rotation profile of the disc, as well as generic field (poloidal and toroidal) configuration of the magnetosphere.

As in plane-parallel flows, the interface modes are mainly driven unstable by the RT and KH instabilities. Toroidal magnetic field tends to suppress the instabilities through magnetic tension. The magnetic field also indirectly affects the RT instability by modifying the effective gravity. Except for the $m = 1$ mode, for which the two opposite effects of B_ϕ cancel (as conjectured by Li & Narayan 2004), we find that increasing B_ϕ generally tends to reduce the growth rates of the interface modes. Differential rotation (with finite vorticity) also tends to suppress the interface instability. To overcome this suppression effect, the disc must have sufficiently large temperature (sound speed) (see Tsang & Lai 2009b). General relativity (GR) can significantly affect the growth rate of interface modes because the disc rotation near the ISCO has smaller vorticity in GR than in Newtonian theory.

Another qualitatively new finding of this paper is that corotation resonance can significantly influence the interface instabilities. As the toroidal field strength in the magnetosphere or in the disc increases, the real frequency of the interface mode falls below $m\Omega_d$ (where Ω_d is the disc rotation rate at the interface), and corotation resonance (or its generalization to magnetic resonances) appears in the disc. Wave absorption at corotation can then significantly change the interface mode growth rate (see Figs. 4, 7, 9).

5.2 Inertial-Acoustic Modes of relativistic Disc

Our model system (Fig. 1) also accommodates inertial-acoustic modes (p-modes) of relativistic discs. These modes are driven unstable primarily by wave absorption at corotation resonance. The magnetosphere-disc interface naturally serves as the inner boundary for the disc. Our study in this paper complements our previous works (Lai & Tsang 2009; Tsang & Lai 2009c; Fu & Lai 2011a) by properly treating the inner boundary condition for disc oscillations. Our result shows that the magnetosphere behaves as a robust “reflector” for spiral waves in the disc: The p-mode frequency and growth rate do not depend sensitively on the property (density, magnetic field) of the magnetosphere. In agreement with Fu & Lai (2011a), we find that a modest disc toroidal field tends to reduce the growth rate of disc p-modes.

5.3 Implications for High-Frequency QPOs in X-ray Binaries

The large-scale ($m = 1, 2, 3, \dots$), overstable oscillation modes studied in this paper may provide an explanation for the high-frequency QPOs observed in NS and BH X-ray binaries (see Section 1). Obviously, the simplicity of our model setup precludes detailed comparison with the phenomenology of QPOs. But we note the following relevant features of disc inertial-acoustic modes and interface modes.

(1) The disc inertial-acoustic modes have frequencies $\omega = \beta_d m \Omega_d$ (with Ω_d the disc rotation rate at r_{in}), with $\beta_d < 1$ (typically ~ 0.5) depending on model parameters (such as disc sound speed) and boundary conditions. If the inner disk is located at the ISCO, the mode frequencies can be computed *ab initio*, and the results are generally consistent with the observations of the HFQPOs in black-hole X-ray binaries (see Lai & Tsang 2009; Tsang & Lai 2009c). The problem with these modes is that even a weak (sub-thermal) disc toroidal magnetic field can suppress their instabilities (see Section 4 and Fu & Lai 2011a). Although large-scale poloidal fields can enhance the instability under certain conditions (see Tagger & Pallet 1999; Tagger & Varniere 2006), it is not clear at this point which effects (disc toroidal field vs large-scale poloidal field) will dominate.

(2) The interface modes have frequencies $\omega = \beta_i m \Omega_d$, with $\beta_i \sim 1$. If $r_{\text{in}} \simeq r_{\text{ISCO}}$, the implied QPO frequencies would be too high compared to observations. Of course, as discussed before (see Sections 1 and 4.3), it is certainly possible that r_{in} is somewhat larger than r_{ISCO} in real systems, but then we would lose the predictive power of our calculations (since in our model r_{in} is a free parameter). On the other hand, the interface modes are robustly unstable, driven by the RT and KH instabilities, and by the corotation effect, especially when the GR effect is included. In most cases, the growth rates of the interface modes are much larger than the disc modes.

Overall, the results of this paper suggest that if the real accreting NS or BH systems can be approximated by our magnetosphere-disc model, the interface oscillations are more likely than inertial-acoustic oscillations to provide an explanation for the observed QPOs. This is reasonable for NS systems, and is consistent with spectral analysis of kHz QPOs in NS X-ray binaries (e.g., Gilfanov et al. 2003). For BH systems, this would require that the inner disc radius in the “transitional state” to be slightly larger than r_{ISCO} (e.g., Done et al. 2007; Oda et al. 2010).

Nevertheless, it should be noted that our calculations of global disc modes are based on a fairly primitive model. Several potentially important physical ingredients have been neglected in our setup, such as finite vertical wavenumber, disc turbulence due to MRI, radial mass inflow across ISCO, etc.. The effects of these factors on our results are certainly worth future investigations. Plus, the disc modes in our study are all linear modes which in principle become nonlinear eventually. Whether our results here are still valid during the nonlinear stage or not needs to be addressed by doing numerical simulations (Fu & Lai 2012, in prep.). Moreover, we have not done any analysis regarding to how these global modes would manifest themselves

observationally. In this sense, our study should better be treated as a demonstration of interesting physical mechanisms, rather than a mature theoretical tool for explaining or predicting HFQPO observations.

ACKNOWLEDGEMENTS

We thank Prof. Wlodek Kluzniak for his careful reading of our manuscript and his valuable suggestions that helped improve our presentation. This work has been supported in part by NSF Grant AST-1008245 and NASA Grant NASA NNX10AP19G. WF also acknowledges the support from a Laboratory Directed Research and Development Program at LANL.

REFERENCES

- Abramowicz M. A., Kluzniak, W. 2001, *A&A*, 374, L19
 Altamirano D., Belloni T., 2012, *ApJL*, 747, L4
 Altamirano D., Belloni T., Linares M., et al., 2011, *ApJL*, 742, L17
 Arras P., Blaes O.M., Turner N. J., 2006, *ApJ*, 645, L65
 Bachetti M., et al., 2010, *MNRAS*, 403, 1193
 Belloni T. M., Motta S. E., Munoz-Darias T., 2011, *BASI*, 39, 409
 Bisnovatyi-Kogan G. S., Ruzmaikin A. A., 1974, *Ap&SS*, 28, 45
 Bisnovatyi-Kogan G. S., Ruzmaikin A. A., 1976, *Ap&SS*, 42, 401
 Chandrasekhar S., 1961, *Hydrodynamic and Hydromagnetic Stability*, Oxford University Press, Oxford
 Done C., Gierlinski M., Kubota A., 2007, *Astron. Astrophys. Rev.*, 15, 1
 Drazin P. G., Reid W. H., 1981, *Hydrodynamic Stability*, Cambridge Univ. Press, Cambridge
 Ferreira B. T., Ogilvie G. I., 2008, *MNRAS*, 386, 2297
 Fu W., Lai D., 2009, *ApJ*, 690, 1386
 Fu W., Lai D., 2011a, *MNRAS*, 410, 399
 Fu W., Lai D., 2011b, *MNRAS*, 410, 1617
 Fu W., Lai D., 2011c, *MNRAS*, 413, 2207
 Fu W., Lai D., 2012, in prep.
 Ghosh P., Lamb, F. K., 1978, *ApJ*, 223, L83
 Gilfanov M., Revnivtsev M., Molkov S., 2003, *A&A*, 410, 217
 Igumenshchev I. V., Narayan R., Abramowicz M. A., 2003, *ApJ*, 592, 1042
 Ikhsanov N. R., Pustil'nik L. A., 1996, *A&A*, 312, 338
 Kato S., 2001, *PASJ*, 53, 1
 Kato S., 2003a, *PASJ*, 55, 257
 Kato S., 2003b, *PASJ*, 55, 801
 Kato S., 2008, *PASJ*, 60, 111
 Kato S., 2011a, *PASJ*, 63, 125
 Kato S., 2011b, *PASJ*, 63, 861
 Kato S., Fukue J., Mineshige S., 2008, *Black-Hole Accretion Disks*, Kyoto Univ. Press, Kyoto
 Kluzniak W., Abramowicz M. A., 2002, *astro-ph/0203314*
 Kulkarni A. K., Romaonva M. M., 2008, *MNRAS*, 386, 673
 Lai D., Tsang D., 2009, *MNRAS*, 393, 979
 Li L., Goodman J., Narayan R., 2003, *ApJ*, 593, 980
 Li L.-X., Narayan R., 2004, *ApJ*, 601, 414
 Lovelace R. V. E., Turner L., Romanova M. M., 2009, *ApJ*, 701, 225
 Lovelace R. V. E., Romanova M. M., Newman W. I., 2010, *MNRAS*, 402, 2575
 Lubow S. H., Spruit, H. C., 1995, *ApJ*, 445, 337
 McKinney J. C., Tchekhovskoy A., Blandford R. D., 2012, *arXiv:1201.4163*
 Miller M. C., Lamb F. K., Psaltis D., 1998, *ApJ*, 508, 791
 Nowak M. A., Wagoner R. V., 1991, *ApJ*, 378, 656
 Oda H., et al., 2010, *ApJ*, 712, 639
 Okazaki A. T., Kato S., Fukue J., 1987, *PASJ*, 39, 457
 Paczynski B., Witta P. J., 1980, *A&A*, 88, 23
 Press W. H., Teukolsky S. A., Vetterling W. T., Flannery B. P., 1992, *Numerical Recipes*. Cambridge Univ. Press, Cambridge
 Rebusco P., Moskalik P., Kluzniak W. et al., 2012, *arXiv:1202.0483*
 Remillard R. A., McClintock J. E., 2006, *ARA&A*, 44, 49

- Reynolds C. S., Miller M. C., 2009, ApJ, 692, 869
 Romanova M. M., Kulkarni A. K., Lovelace R. V. E., 2008, ApJ, 673, L171
 Rothstein D. M., Lovelace R. V. E., 2008, ApJ, 677, 1221
 Spruit H. C., Stehle R., Papaloizou J. C. B., 1995, MNRAS, 275, 1223
 Stella L., Vietri M., Morsink S. M. 1999, ApJ, 524, L63
 Swank J., 1999, Nuclear Phys. B, Proc. Suppl., 69, 12
 Tagger M., Pellat R. 1999, A&A, 349, 1003
 Tagger M., Varniere P. 2006, ApJ, 652, 1457
 Tsang D., Lai D., 2008, MNRAS, 387, 446
 Tsang D., Lai D., 2009a, MNRAS, 393, 992
 Tsang D., Lai D., 2009b, MNRAS, 396, 589
 Tsang D., Lai D., 2009c, MNRAS, 400, 470
 van der Klis M., 2006, in Lewin W. H. G., van der Kils M., eds, Compact Stellar X-ray sources. Cambridge Univ. Press, Cambridge
 Wagoner R. V., 1999, Phys. Rep., 311, 259

APPENDIX A: GENERAL MAGNETIC FIELD PROFILES IN THE MAGNETOSPHERE

In the main text of this paper we adopt a special toroidal magnetic field profile $B_\phi \propto r$ in the magnetosphere so that the perturbation equations have simple analytical solutions. For a more general magnetic field profile $B_\phi \propto r^q$, with $q > 1$, analytical solutions are no longer attainable, and we must solve numerically the perturbation equations for both the disc (Eqs. [22]-[23]) and the magnetosphere (Eqs. [9]-[10]). To this end, we first need to derive the boundary condition at the the inner boundary of the magnetosphere, which is close to the center of the system ($r = 0$). This is done by requiring the solutions to be regular at small radius. As $r \rightarrow 0$, we observe that $\omega_{A\phi} \propto B_\phi/r \rightarrow 0$. In this limit, Eqs. (9)-(10) then reduce to

$$\frac{d\xi_r}{dr} = -\frac{1}{r} \frac{\tilde{\omega} - 2m\Omega}{\tilde{\omega}} \xi_r + \frac{m^2}{r^2} \delta h, \quad (\text{A1})$$

$$\frac{d\delta h}{dr} = (\tilde{\omega}^2 - r\Omega^2) \xi_r + \frac{2m\Omega}{r\tilde{\omega}} \delta h, \quad (\text{A2})$$

i.e, recovering the hydrodynamic equations¹. These simplified equations can be readily solved, leading to a relation between ξ_r and δh :

$$\xi_r = \frac{m\delta h}{r\tilde{\omega}(\tilde{\omega} + 2\Omega)}. \quad (\text{A3})$$

With this regularity condition implemented at some finite yet small inner boundary r_c , we carry out the integration in the magnetosphere towards the interface, while at the same time we also integrate the disc equations towards the same interface and employ shooting procedure to solve for the eigenvalues by requiring solutions from both regions satisfy the matching condition at the interface (i.e., continuity of ξ_r and $\Delta\Pi$). Note that the eigenvalues of the system now have two components: the wave frequency ω , and the relation between the solutions in two regions, e.g., $\delta h(r_c)/\delta h(r_{\text{out}})$ or $\xi_r(r_c)/\xi_r(r_{\text{out}})$.

APPENDIX B: PLANE-PARALLEL FLOW WITH A COMPRESSIBLE UPPER LAYER AND A MAGNETIZED LOWER LAYER

Consider a system with two separate fluid layers in a constant gravitational field $\mathbf{g} = -g\hat{z}$. The upper layer ($z > 0$) is a compressible fluid of density $\rho = \rho_+ e^{-z/H_z}$ and constant horizontal velocity u_+ , and the lower layer ($z < 0$) is an incompressible fluid of constant density ρ_- and horizontal velocity u_- . Here, $H_z = c_s^2/g$ is the density scale height with c_s being the sound speed, and both velocities are along the x -axis. This system was studied by Tsang & Lai (2009b), but here we add a uniform horizontal magnetic field B_x in the lower fluid. As in Tsang & Lai (2009b) (correcting typos in their Appendix), we apply perturbations of the form $e^{ikx - i\omega t}$ to both layers and solve for ω by demanding the Lagrangian displacement and Lagrangian total pressure perturbation be continuous across the interface between upper and lower fluids. Denoting

$$\tilde{\omega}_+ = \omega - ku_+,$$

$$k_z^2 = (k^2 - \tilde{\omega}_+^2/c_s^2),$$

¹ See Fu & Lai (2011c) for the derivation of the regularity condition for a even more general system (differentially rotating, magnetized, self-gravitating, etc.).

$$\tilde{k} = (\sqrt{1 + 4H_z^2 k_z^2} - 1)/2H_z,$$

and

$$\tilde{\rho}_+ = \rho_+ k / \tilde{k},$$

the final solution for ω can be written as

$$\omega = \frac{k(\tilde{\rho}_+ u_+ + \rho_- u_-)}{\tilde{\rho}_+ + \rho_-} \pm \sqrt{-\frac{k^2(u_+ - u_-)^2 \tilde{\rho}_+ \rho_-}{(\tilde{\rho}_+ + \rho_-)^2} - \frac{kg(\rho_+ - \rho_-)}{\tilde{\rho}_+ + \rho_-} + \frac{k^2 B_x^2}{4\pi(\tilde{\rho}_+ + \rho_-)}}. \quad (\text{B1})$$

The three terms under the square root clearly have different physics meanings. The first term signifies the Kelvin-Helmholtz instability which disappears when velocity shear across the interface vanishes; the second term depicts the Rayleigh-Taylor instability which only exists for non-zero density contrast; the last term, the only difference between Eq. (B1) and Eq. (A14) in Tsang & Lai (2009b), describes the stabilizing effect of the magnetic field that lies along the direction of the perturbation wave vector. If we take the incompressible and hydrodynamic limit (i.e., $c_s \rightarrow \infty$, $H_z \rightarrow \infty$ so that $\tilde{k} \rightarrow k$, $\tilde{\rho}_+ \rightarrow \rho_+$, and $B_x \rightarrow 0$), then the above equation reduces to Eq. (B12) in Li & Narayan (2004).

